Fluid Dynamics & Materials Processing FDMP, vol.16, no.1, pp.21-30, 2020

A Study on the Reduction of the Aerodynamic Drag and Noise Generated By the Roof Air Conditioner of High-Speed Trains

Jiali Liu[1], Mengge Yu[2,*], Dawei Chen[1] and Zhigang Yang[3]

Abstract: In order to investigate how the aerodynamic drag and noise produced by the roof air conditioner of a high-speed train can be reduced, the related unsteady flow in the near-field was computed using the method of large eddy simulation. In this way, the aerodynamic source for noise generation has initially been determined. Then, the far-field aerodynamic noise has been computed in the framework of the Lighthill's acoustics analogy theory. The propulsion height and flow-guide angle of the roof air conditioner were set as the design variables. According to the computational results, a lower propulsion height or flow-guide angle is beneficial in terms of aerodynamic drag and noise mitigation. However, compared to the design scheme with propulsion height of 0mm, the aerodynamic drag coefficient of the configuration with propulsion height of 190mm and flow-guide angle of 30° is slightly larger, while the aerodynamic noise is obviously reduced. Thus, from the viewpoint of the aerodynamic drag and noise, the design scheme with propulsion height of 190 mm and flow-guide angle of 30° is the optimal configuration in the range of conditions examined in the present work.

Keywords: Aerodynamic drag, aerodynamic noise, roof air conditioner, large eddy simulation, acoustics analogy theory.

1 Introduction

With the increasing of train speed, the aerodynamic effects of the high-speed train become more and more significant, and the aerodynamic performance of the high-speed train running on the open track has become the main factor to restrain the development of the high-speed train [Yu, Zhang, Zhang et al. (2014); Zhu (2015)]. The aerodynamic drag is proportional to the square of the train speed. When the train speed reaches 300 km/h, the aerodynamic drag could take 75% of the total resistance. The aerodynamic noise is proportional to the 6~8 power of the train speed. When the train speed reaches 300 km/h, the aerodynamic noise will exceed the wheel/rail noise and become the main noise of the high-speed train [Thompson, Latorre Iglesias, Liu et al. (2015)]. The reduction of the aerodynamic drag and noise of the high-speed train is of great importance to the

[1] CRRC Qingdao Sifang Co., Ltd., Qingdao, 266111, China.

[2] College of Mechanical and Electronic Engineering, Qingdao University, Qingdao, 266071, China.

[3] School of Traffic & Transportation Engineering, Central South University, Changsha, 410075, China.

[*] Corresponding Author: Mengge Yu. Email: yumengge0627@163.com.

Received: 07 June 2019; Accepted: 15 August 2019.

aerodynamic design of the high-speed train. The aerodynamic drag and noise can be reduced by the optimization of the streamlined head [Yu, Zhang, Zhang et al. (2013); Yao, Guo and Yang (2012)]. Furthermore, the non-smooth parts on the train body also have great influence on the aerodynamic drag and noise of the high-speed train. Tan et al, Zhang et al. established the computational method of the aerodynamic noise radiated from the pantograph of the high-speed train and studied the aerodynamic noise characteristics of the pantograph [Tan, Yang, Tan et al. (2018), Zhang, Zhang, Li et al. (2017)]. Cui et al. studied the aerodynamic noise radiated from the connection position of the high-speed train [Cui, Tian and Zhao (2017)]. Huang et al. investigated various design schemes so as to reduce the aerodynamic drag of the high-speed train by the wind tunnel test, and found that the roof air conditioner fairing, pantograph fairing, bogie apron board and full-enclosed windshield can reduce the aerodynamic drag of the high-speed train [Huang, Chen and Jiang (2012)]. The roof air conditioner is the main non-smooth part on the train body surface. The propulsion height and flow-guide angle of the roof air conditioner are important design parameters, which have much influence on the aerodynamic drag and noise of the high-speed train. At present, there are no detailed studies for the design of the propulsion height and flow-guide angle of the roof air conditioner. Therefore, in the present paper, the computational methods of the aerodynamic drag and noise of the high-speed train are established, and the influences of the propulsion height and flow-guide angle of the roof air conditioner on the aerodynamic drag and noise of the high-speed train are studied.

2 Governing equations

At present, the best approach to simulate aerodynamic noise is to divide the computational domain into two parts: one part is used to describe the nonlinear generation progress of the sound, which is called the near-field; the other part is used to describe the linear propagation process of the sound, which is called the far-field. The near-field is usually computed by the large eddy simulation (LES) in order to investigate the exact unsteady flow field information, and obtain the exact aerodynamic noise source. The far-field is usually computed by the Lighthill's acoustics analogy theory, through which the aerodynamic noise radiated from the aerodynamic noise source can be computed quickly and accurately.

2.1 Large eddy simulation

For the LES, the mathematical filter function should firstly be established to filter the eddy whose scale is smaller than the filter function. Then the additional stress term should be introduced to reflect the influence of the small scale eddy on the motion of the large scale eddy. The velocity of the large scale eddy is defined as the filtered velocity [Hodor, Birle, Nascutiu et al. (2017)],

$$\overline{u}_i(\mathbf{x},t)=\int G(\mathbf{x},\mathbf{x}',\mathbf{\Delta})u_i(\mathbf{x}',t)d\mathbf{x}' \tag{1}$$

where, $\overline{u}_i$ is the filtered velocity; u_i is the velocity; G is the filter function, which is used to calibrate the large scale eddy and filter the small scale eddy; $\mathbf{x}$, $\mathbf{x}'$ are the Cartesian coordinate vector, respectively; $\mathbf{\Delta}$ is the filter length vector; t is the time. The filter

operation and derivation operation can be exchanged, the following equations can be obtained when the filtering function is applied to the Navier-Stokes equations,

$$\frac{\partial \overline{u}_i}{\partial x_i} = 0 \tag{2}$$

$$\frac{\partial \overline{u}_i}{\partial t} + \frac{\partial \overline{u}_i \overline{u}_j}{\partial x_j} = -\frac{1}{\rho}\frac{\partial \overline{p}}{\partial x_i} + \frac{\mu}{\rho}\frac{\partial^2 \overline{u}_i}{\partial x_j \partial x_j} + \frac{\partial \overline{\tau}_{ij}}{\partial x_j} \tag{3}$$

where, ρ is the density; $\overline{p}$ is the filtered pressure; μ is the shear coefficient of viscosity;

$$\overline{\tau}_{ij} = -\left(\overline{u_i u_j} - \overline{u}_i \overline{u}_j\right) \tag{4}$$

where, $\overline{\tau}_{ij}$ are the sub-grid scale (SGS) stresses, which are unknown and must be modeled. In the present paper, the Smagorinsky model is used, which models the SGS stresses as,

$$\overline{\tau}_{ij} - \frac{1}{3}\overline{\tau}_{kk}\delta_{ij} = -2\mu_t \overline{S}_{ij} \tag{5}$$

where, δ_{ij} is the Kronecker delta; μ_t is the subgrid turbulent viscosity coefficient, $\overline{S}_{ij}$ is the resolved rate of strain, which is defined as

$$\overline{S}_{ij} = \frac{1}{2}\left(\frac{\partial \overline{u}_i}{\partial x_j} + \frac{\partial \overline{u}_j}{\partial x_i}\right) \tag{6}$$

2.2 Acoustics analogy theory

In 1952, Lighthill proposed the Lighthill equation by the acoustic analogy method. However, the Lighthill equation was derived in the free space without considering the influence of the wall boundary. In 1969, Ffowcs Williams and Hawkings considered the influence of the wall boundary on the sound and proposed the FW-H equation [Ffowcs Williams and Hawkings (1969)]. To solve the FW-H equation, various acoustic integral formulas were proposed, and the porous KFW-H integral formula was widely used. In the KFW-H integral formula, the sound pressure $p'(\mathbf{x},t)$ at the far-field measuring point $\mathbf{x}$ can be expressed as [di Francescantonio (1997)]:

$$p'(\mathbf{x},t) = p'_M(\mathbf{x},t) + p'_D(\mathbf{x},t) + p'_Q(\mathbf{x},t) \tag{7}$$

where

$$p'_M(\mathbf{x},t) = \frac{1}{4\pi}\int_{f=0}\left[\frac{\rho_0\left(\dot{U}_n + U_{\dot{n}}\right)}{r\left(1-M_r\right)^2}\right]\mathrm{d}S + \frac{1}{4\pi}\int_{f=0}\left[\frac{\rho_0 U_n\left\{r\dot{M}_r + a_0\left(M_r - M^2\right)\right\}}{r^2\left(1-M_r\right)^3}\right]\mathrm{d}S \tag{8}$$

$$p'_D(\mathbf{x},t)=\frac{1}{4\pi}\int_{f=0}\left[\frac{\dot{L}_r}{a_0 r(1-M_r)^2}\right]\mathrm{d}S+\frac{1}{4\pi}\int_{f=0}\left[\frac{L_r-L_M}{r^2(1-M_r)^2}\right]\mathrm{d}S$$
$$+\frac{1}{4\pi}\int_{f=0}\left[\frac{L_r\{r\dot{M}_r+a_0(M_r-M^2)\}}{a_0 r^2(1-M_r)^3}\right]\mathrm{d}S \tag{9}$$

where,

$$U_i=v_i+\frac{\rho}{\rho_0}(u_i-v_i) \tag{10}$$

$$L_i=p_{ij}\hat{n}_j+\rho u_i(u_n-v_n) \tag{11}$$

where, $p'_M(\mathbf{x},t)$, $p'_D(\mathbf{x},t)$, $p'_Q(\mathbf{x},t)$ are the thickness noise, load noise, quadrupole noise, respectively; Under subsonic condition, the value of $p'_Q(\mathbf{x},t)$ is very small, which can be ignored. The meanings of the variables in Eqs. (8)-(11) were described specifically in the di Francescantonio [di Francescantonio (1997)], which are not given in the present paper.

3 Numerical model

3.1 Computational domain and mesh

Numerical wind tunnel method is used in the present paper, and the computational domain is shown in Fig. 1. The size of the computational domain is 400 m×30 m×20 m. The boundary ABCD is set as the velocity inlet boundary, the boundary EFGH is set as the pressure outlet boundary. The boundaries BFGC, AEHD and CGHD are set as the symmetry boundary. The bottom boundary ABFE is set as the slip wall boundary, which has the same speed with the freestream. The train is set as the no-slip wall boundary.

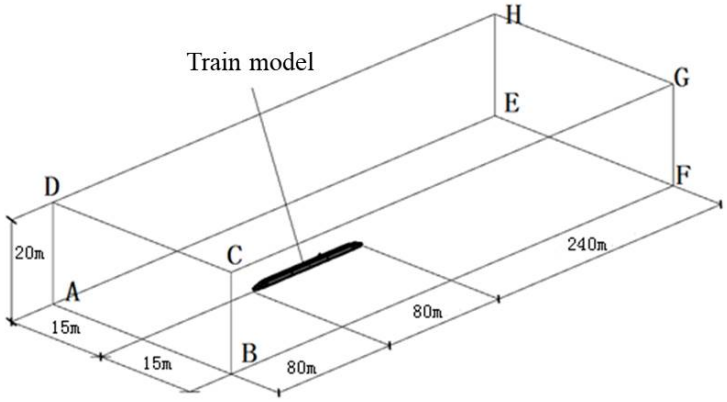

Figure 1: Computational domain

The mesh should meet basic requirements concerning wall units adjacent to no-slip walls, appropriate for the selected computational method and turbulence model. In the method of LES, the typical value for the dimensionless wall distance y^+ of the first cell layer should be around 1. The computational mesh is shown in Fig. 2. The triangular meshes

are generated on the train surface, and the tetrahedral meshes are generated in the computational domain. As for the mesh size, the maximum surface sizes of the streamlined head, car body of head and tail, middle car, and bogies are 40 mm, 60 mm, 80 mm, and 40 mm, respectively. The height of the first cell off the wall is 0.1 mm, and the total number of boundary layers is 20. This sizing makes y^+ on the train around 1, which satisfies the requirement of the turbulent computation. The total number of the mesh is about 60 million.

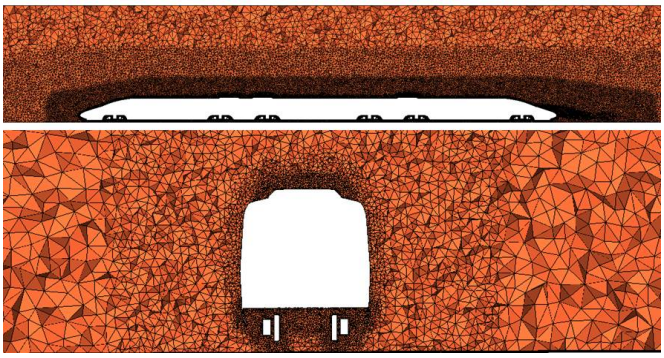

Figure 2: Computational mesh

For the steady flow field computation, the Realizable k-ε model is used to simulate the turbulent effect. The SIMPLE algorithm is chosen for the pressure-velocity coupling. For the spatial discretization, the pressure term is discretized using the standard scheme, and the momentum and turbulent terms are discretized using the second order upwind scheme. For the unsteady flow field computation, the steady flow field is set as the initial flow field. The LES is used to simulate the turbulent effect, and the PISO algorithm is chosen for the pressure-velocity coupling. For the spatial discretization, the pressure term is discretized using the PRESTO! scheme, and the momentum terms are discretized using the bounded central difference scheme. The time step is 5×10^{-5} s, and the total time step size is 10000.

3.2 Computational case and measuring points

The roof air conditioner of the high-speed train is rectangular in shape. The propulsion height and flow-guide angle of the roof air conditioner have much influence on the aerodynamic drag and noise of the high-speed train, thus, they are chosen as design variables in the present paper. Fig. 3 shows a schematic diagram of the propulsion height and flow-guide angle of the roof air conditioner. Without changing the length and width of the air conditioner, 3 kinds of propulsion heights (190 mm, 250 mm, 350 mm) and 4 kinds of flow-guide angles (30°, 45°, 60°, 90°) are considered in the present paper. The propulsion height of 0 mm is also considered for comparison. A total of 13 computational cases are studied in the present paper. In addition, it is important to note that, the height of the train body should be adjusted to ensure that the height between the top of the air conditioner and the top of the rail has no change.

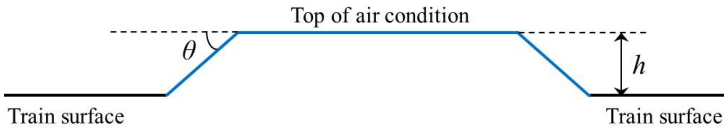

Figure 3: Design scheme of the air conditioner

The far-field measuring points are arranged along the operational direction of the train, which are 25 m far away from the center of the track and 3.5 m above the top of the rail. There are 16 measuring points, and the first point is 20m in front of the streamlined head nose, as shown in Fig. 4. The origin is located at the streamlined head nose, thus the x coordinates of the measuring points are from -20 m (corresponding to measuring point 1) to 130 m (corresponding to measuring point 16). The train is located between the measuring point 3 and measuring point 11.

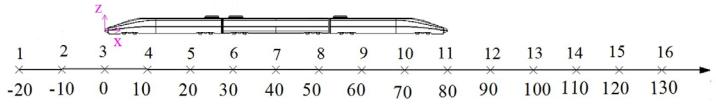

Figure 4: Far-field measuring points

3.3 Computation verification

In the present paper, the aerodynamic noise radiated from the cylinder is computed, and the computational result is compared with the test result in order to verify the accuracy of the computational method. Fig. 5 shows the frequency spectrum of aerodynamic noise in terms of comparison between computation and test.

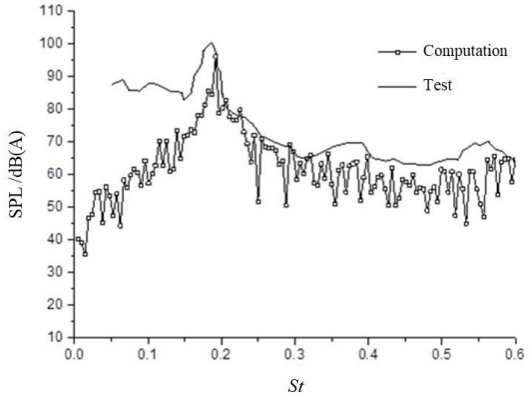

Figure 5: Comparison of computational and test results

As shown in Fig. 5, the computational result is in good agreement with the test result, thus the computational method in the present paper is reliable.

4 Computational results analysis

4.1 Aerodynamic drag

Fig. 6 shows the pressure counter on the train surface for some typical computational cases. In order to have a clearer understanding the pressure variation characteristics on

the roof air conditioner, the pressure counter on the first roof air conditioner is also given in each figure. It can be seen from Fig. 6 that, with the increasing of the flow-guide angle of the roof air conditioner, both the positive pressure on the windward side and the negative pressure on the leeward side of the roof air conditioner increase, which could lead to the increasing of the aerodynamic drag of the high-speed train. Thus, the decrease of flow-guide angle contributes to the reduction of the aerodynamic drag of the high-speed train. Similar pressure variation rules can be obtained when increasing the propulsion height of the roof air conditioner, which indicates that reducing propulsion height of the roof air conditioner is beneficial for the reduction of the aerodynamic drag of the high-speed train. Therefore, from the viewpoint of aerodynamic drag, the design scheme with small flow-guide angle or low propulsion height seems to be optimal.

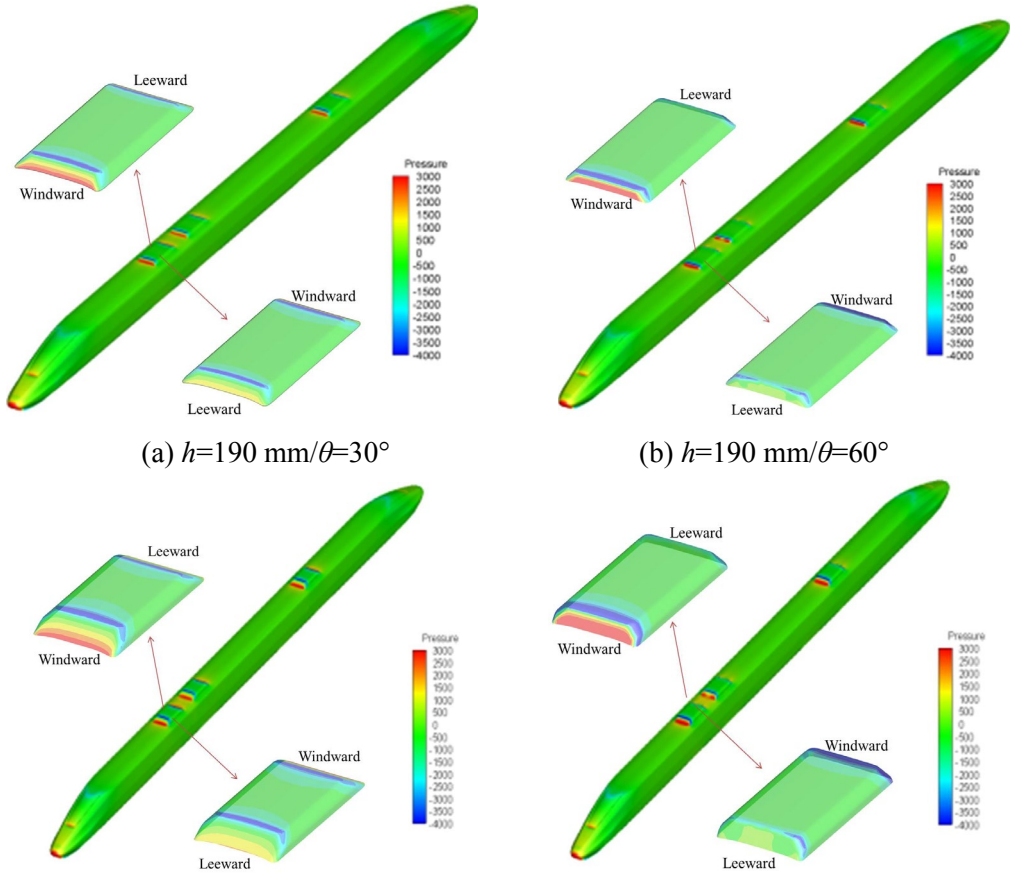

(a) h=190 mm/θ=30° (b) h=190 mm/θ=60°

(c) h=350 mm/θ=30° (d) h=350 mm/θ=60°

Figure 6: Pressure counter on the train surface

Tab. 1 shows the aerodynamic drag coefficient of the high-speed train for various flow-guide angles and propulsion heights. It can be seen from Tab. 1 that, with the increasing of the propulsion height h, the aerodynamic drag coefficient of the high-speed train increases. The aerodynamic drag coefficient has a minimum value when h=190 mm and θ=30°, and a

maximum value when h=350 mm and θ=90°. In addition, for the design scheme of h=0 mm, the aerodynamic drag coefficient is slightly smaller compared to the design scheme of h=190 mm and θ=30°, and the difference is less than 1%. Therefore, in order to reduce aerodynamic drag of the high-speed train, if the space allows, the air conditioner can completely sink, i.e., the propulsion height is 0 mm. If the space is limited, the air conditioner can partly sink with smaller flow-guide angle or lower propulsion height.

Table 1: Aerodynamic drag force coefficient

	θ=30°	θ=45°	θ=60°	θ=90°
h=190 mm	0.316	0.321	0.326	0.324
h=250 mm	0.327	0.329	0.337	0.338
h=350 mm	0.336	0.342	0.342	0.349

4.2 Aerodynamic noise

In order to study the spectral characteristics of the aerodynamic noise of the high-speed train, the measuring point 7, corresponding to the middle of the train, is taken as an example. Fig. 7 shows the frequency spectrum of the far-field aerodynamic noise of the measuring point 7 for some typical computational cases. It can be seen from Fig. 7 that, with the increasing of the frequency, the sound pressure level increases first, and then decreases. The aerodynamic noise has a wide range of spectrum, and the main energy is concentrated around 1000 Hz. With the increasing of the propulsion height, the sound pressure level has a rising tendency within the scope of medium and high frequencies. Of all the design schemes simulated in the present paper, the sound pressure level has a relatively small value when h=190 mm and θ=30°. As for the other measuring points, the aerodynamic noises have similar spectral characteristics.

Fig. 8 shows the comparison of the total sound pressure levels at all frequencies of each measuring point between design scheme of h=190 mm/θ=30° and design scheme of h=0 mm. It can be seen from Fig. 8 that, compared to the design scheme with propulsion height of 0 mm, the aerodynamic noise of the one with propulsion height of 190 mm and flow-guide angle of 30° is obviously reduced, nevertheless, the aerodynamic drag is slightly increased as described in Section 4.1. Therefore, from the viewpoint of the aerodynamic drag and noise, the design scheme with propulsion height of 190 mm and flow-guide angle of 30° is optimal in the research conditions of the present paper.

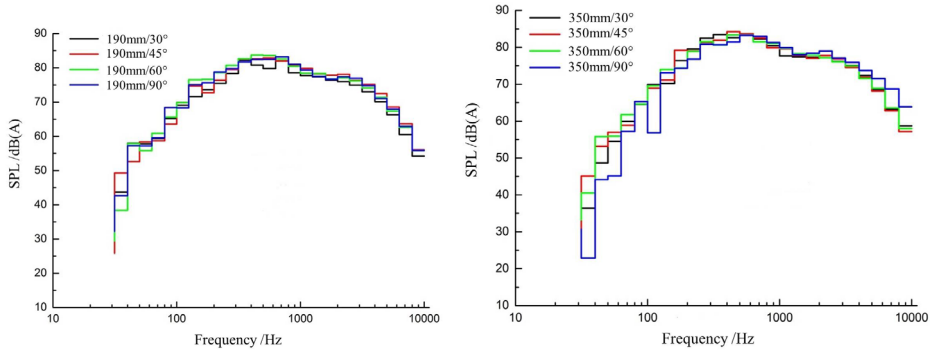

(a) h=190 mm (b) h=350 mm

Figure 7: Frequency spectrum of the far-field aerodynamic noise

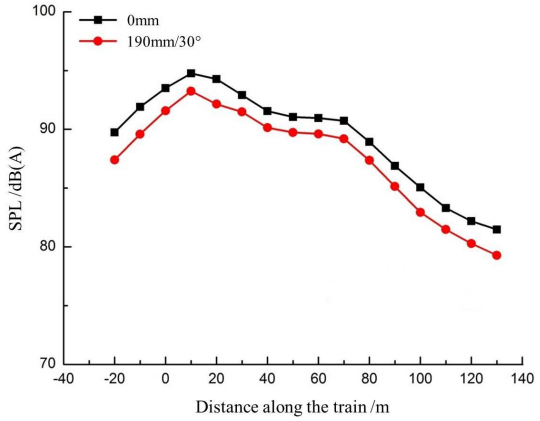

Figure 8: Comparison of sound pressure level

5 Conclusions

The roof air conditioner is the main non-smooth part on the train body surface. The propulsion height and flow-guide angle of the roof air conditioner are important design parameters, which has much influence on the aerodynamic drag and noise of the high-speed train. In the present paper, the influence of the design schemes of the roof air conditioner on the aerodynamic drag and noise of the high-speed train was studied based on the LES and Lighthill's acoustic analogy theory. According to the simulation results and analysis above, the conclusions are as follows:

(1) Based on the pressure distribution of the train, the design scheme with smaller flow-guide angle and lower propulsion height is optimal. If the space allows, the air conditioner can completely sink from the perspective of aerodynamic drag.

(2) With the increasing of the frequency, the sound pressure level has a tendency to first increase and then decrease, and the main energy is concentrated around 1000 Hz.

(3) From the perspective of both aerodynamic drag and aerodynamic noise, the design scheme with the propulsion height of 190 mm and flow-guide of 30° is optimal.

Acknowledgement: The paper is supported by the National Key R & D Program of China (No. 2016YFB1200504-F), the National Natural Science Foundation of China (No. 51705267), the China Postdoctoral Science Foundation (No. 2018M630750) and the China Railway R & D Program (No. 2015J009-D).

Conflicts of Interest: The authors declare that they have no conflicts of interest to report regarding the present study.

References

Cui, Y.; Tian, C.; Zhao, Z. (2017): Research on the radiation characteristics of aerodynamic noises in the connection position of high-speed trains. *Journal of Vibroengineering*, vol. 19, no. 4, pp. 3099-3112.

di Francescantonio, P. (1997): A new boundary integral formulation for the prediction of sound radiation. *Journal of Sound and Vibration*, vol. 202, no. 4, pp. 191-509.

Ffowcs Williams, J. E.; Hawkings, D. L. (1969): Sound generation by turbulence and surfaces in arbitrary motion. *Philosophical Transactions for the Royal Society of London, Series A, Mathematical and Physical Sciences*, vol. 264, no. 1151, pp. 321-342.

Hodor, V.; Birle, D.; Nascutiu, L.; Deac, I. (2017): Aeroacoustics-noise prediction by using "LES" for signal processing. *Energy Procedia*, vol. 112, pp. 322-329

Huang, Z. X.; Chen, L.; Jiang, K. L. (2012): Wind tunnel test of air-drag reduction schemes of high-speed trains. *Journal of the China Railway Society*, vol. 34, no. 4, pp. 16-21 (In Chinese).

Thompson, D. J.; Latorre Iglesias, E.; Liu, X.; Zhu, J. Y.; Hu, Z. W. (2015): Recent developments in the prediction and control of aerodynamic noise from high-speed trains. *International Journal of Rail Transportation*, vol. 3, no. 3, pp. 119-150.

Tan, X. M.; Yang, Z. G.; Tan, X. M.; Wu, X. L.; Zhang, J. (2018): Vortex structures and aeroacoustic performance of the flow field of the pantograph. *Journal of Sound and Vibration*, vol. 432, pp. 17-32.

Yao, S. B.; Guo, D. L.; Yang, G. W. (2012): Three-dimensional aerodynamic optimization design of high-speed train nose based on GA-GRNN. *Science China Technological Sciences*, vol. 55, no. 11, pp. 3118-3130.

Yu, M. G.; Zhang, J. Y.; Zhang, W. H. (2013): Multi-objective optimization design method of the high-speed train head. *Journal of Zhejiang University-Science A (Applied Physics & Engineering)*, vol. 14, no. 9, pp. 631-641.

Yu, M. G.; Zhang, J. Y.; Zhang, W. H. (2014): Study on the operational safety of high-speed trains exposed to stochastic winds. *Acta Mechanica Sinica*, vol. 30, no. 3, pp. 351-360.

Zhang, Y. D.; Zhang, J. Y.; Li, T. (2017): Investigation of the aeroacoustic behavior and aerodynamic nose of a high-speed train pantograph. *Science China Technological Sciences*, vol. 60, no. 4, pp. 561-575.

Zhu, J. (2015): *Aerodynamic Noise of High-Speed Train Bogies*. University of Southampton.